Interdisciplinary project: Improvement of the Gauss algorithm for determining orbital parameters from satellite tracks.

Salm Jérémy, Leurent Gauthier, Debons Robin

June 5, 2023

1 Introduction

The conquest of space has fascinated mankind for decades, with ever larger and more far-reaching missions being launched. The objectives of these missions are varied and challenging. The development of modern technology has allowed the development of telescopes, satellites and rockets, each more powerful than the last and leading to major scientific discoveries. For example, on 25 December 2021, the James Webb Telescope is sent into space and takes on the function of an observatory in motion. To name but a few, its main missions will be to study the formation of galaxies and to contribute to a deeper understanding of the atmosphere of exoplanets to better understand the origins of life [1]. Another example is the Meteosat Third Generation Imager-1 (MTG-I1) satellite launched on 13 December 2022. It carries high-tech instruments that will enable images to be obtained with a resolution never before achieved. Its use should lead to a better understanding of severe weather events and the formation of clouds at high altitudes [2].

While these launches of new space objects are useful for understanding current scientific and societal issues, these missions are creating an increase in the number of objects orbiting the Earth. To get an idea of the scale of this phenomenon, the European Space Agency (ESA) makes estimates of the number of objects orbiting the Earth. For example, the number of satellites in orbit is approximately 10'000, of which only 7'600 are still operational. This means that the remaining satellites generate unnecessary danger and pollution of the Earth's orbit. Indeed, the latter can collide with still operational space objects such as other satellites or the International Space Station (ISS) and exponentially increase the number of space debris, which currently stands at around one hundred million according to the same source. Note that only 30'000 space debris have been detected by ESA to date [3]. In addition to the danger they represent, these debris can also disturb the data generated by astrophysical or meteorological observations [4]. Therefore, it is necessary to increase the number of institutions involved in this growing problem.

This work is carried out within *the Space Situation Awareness EPFL team (SSA)*, based at the Federal Institute of Technology in Lausanne (EPFL). It takes place as a improvement of the work done last year in the same association [5]. First of all, it will be a question of making comparisons between some orbital parameters for several satellites obtained during this work with reference values. In particular, the study of their relative errors will be carry out. In addition, the angular variation for different temporal modifications will be examined for some of these parameters. Finally, several cases will be considered by modifying the angles that locate the satellites in order to understand the associated sensitivity.

2 Theoretical background

2.1 Angles convention

There are many different ways of indicating the position of a point in space. However, some are more adapted than others for a given application. In principle, one needs 3 coordinates to fully describes the position of an object, but to point at a star with a telescope, one only needs two angles. The observer does not need to know the distance between the object and the telescope, hence the third spatial freedom degree is not needed anymore. The sky the observer sees can be interpreted as the projection of the universe on a sphere with the center at the center of the Earth. This sphere is called the celestial sphere. The two angles used in this work and that are usually used to describe an object in the celestial sphere are the Right Ascension (RA) and the Declination (DEC). These angles are independent of the observer's position on Earth. It is an equatorial system of coordinates which origin is the center of the Earth. To define these two angles, lets first define some other objects of interest.

The plane containing the earth's orbit around the sun is called the ecliptic plane. The equatorial plane is the plane containing the Earth equator. The celestial equator is the projection of the Earth equator on the celestial sphere, such that the celestial equator is the intersection of the equator plane and the celestial sphere. The celestial equator and the ecliptic plane intersect in two points. During an equinox, the sun is on one of this two points. The one at which the sun stands during spring equinox is called the vernal point. This leads to the definition of the two angles RA and DEC : the Right Ascension is the angle measured on the celestial equator from the vernal point to the object on the celestial sphere. It is defined to be positive when increasing to the East. It is the celestial equivalent of the longitude on Earth. The declination is the angle between the celestial equator and the object in the celestial sphere. It is positive in the northern hemisphere, and negative in the southern hemisphere. It is the celestial equivalent of the latitude on Earth.

Finally, the Declination is usually given in degrees, arc-minutes and arc-seconds, and the Right Ascension is usually given in hour-angle, i.e. hours, minutes, seconds. A scheme illustrating the right ascension and the declination is shown in Sect. 7, Fig. 13.

2.2 Two Lines Elements

The final objective of this work is the determination of the satellite's TLE's (Two Line Elements). These form a standardised representation of the orbital parameters of the observed object orbiting the Earth. They all have the same structure which allows organisations studying these objects to use the same convention. It's important to understand that TLE are only valid for a certain period of time (usually a few days) and are calculated regularly in order to constantly have data that correlate with physical reality. Indeed, orbiting objects are subject to a number of perturbations, sometimes irregular, which modify their trajectory [6]. For example, the solar wind and the attraction of the Moon are two phenomena that deviate objects from their initial trajectory. In addition, the TLE's structure is composed of a first line (line 0) giving the character name of the studied objet and a second and third line (line 1 and line 2) describing the different informations about this object. As an example, Fig. 1 shows the TLE for the Starlink-3965 satellite dating from 2 May 2023.

```
0 STARLINK-3965
1 52550U 22051T   23122.44463570  .00001526  00000-0  11391-3 0  9992
2 52550  53.2144 127.9372 0001351  79.3600 280.7544 15.08843732 54105
```

Figure 1: TLE for Starlink-3965 satellite valid during the 2$^{\text{nd}}$ of May 2023 [7].

The descriptions of the different columns of a TLE are presented thanks to Tab. 2a and Tab. 2b which give the content of the line 1 and line 2, respectively.

The most important elements in the reconstruction of an orbit are the inclinaison i, the right ascension of the ascending node Ω, the eccentricity e, the argument of the perigee ω, the mean anomaly M and the mean motion n. The physical meaning of these terms is therefore developed. Firstly, the inclination i represents the angle between the plane of the satellite's orbit and ecliptic plane. Ω is the right ascension of the ascending node. the ascending node is point where the satellite crosses the equatorial plane from north to south. In addition, the eccentricity e describes the difference in shape between the orbit and a circle. The eccentricity is positive. Between $e = 0$ and $e = 1$, the orbit is an ellipse, and is a perfect circle for $e = 0$. For $e > 1$, the described trajectory is a hyperbola, which is not a closed shape anymore. The perigee argument ω is the angle between the direction of the ascending node and the perigee (measured on the plane containing the satellite's orbit), where the perigee is the point in the satellite's orbit closest to the focus of that orbit. The mean anomaly M represents the fraction of the orbital period since the satellite last passed perigee, expressed as an angle. Finally, the mean motion n represents the average angular velocity of the satellite observed in an elliptical orbit.

Columns	descriptions
01	Line number
03-07	Satellite number
08	Classification
10-11	Last two digits of launch year
12-14	Launch number of the year
15-17	Piece of the launch
19-20	Epoch year (Last two digits of year)
21-32	Epoch (Day of the year and fractional portion of the day)
34-43	First time derivative of mean motion
45-52	Second time derivative of mean motion
54-61	BSTAR drag term
63	Ephemeris type
65-68	Element number
69	Checksum (modulo 10)

(a)

Columns	descriptions
01	Line number
03-07	Satellite number
09-16	Inclinaison (degrees)
18-25	Right Ascension of the Ascending Node (degrees)
27-33	Eccentricity
35-42	Argument of Perigee (degrees)
44-51	Mean anomaly (degrees)
53-63	Mean motion (Revolutions per day)
64-68	Revolution number at epoch (Revolutions)
69	Checksum (modulo 10)

(b)

Figure 2: Descriptions of the differents columns of a TLE for (a) line 1, and (b) line 2.

2.3 Code modifications and updates

This work was supposed to use a code previously written, whose purpose is to generate IODs (Interactive orbital determination), which are then taken as parameters by the Gauss algorithm to determine the TLEs [5] (see Sect. 7 for details on IODs). However, the latter shows many problems. First of all, the code was not running in the first place. Some tiny errors were corrected in order to run the code on a test image.

Also, the angles convention that was used in the code was Altitude and Azimuth, which is an azimuthal coordinates system that depends on the position of the observer on Earth. This was not practical because this was leading to a lot of angles conversions. Moreover, the mount is an equatorial one, which makes it much easier to use with an equatorial system of coordinates. Also, the RA and DEC angles are widely used, unlike the Altitude and Azimuth. This has led to several modifications in the code, and everything was then written using Right Ascension and Declination instead of Altitude and Azimuth.

Another improvement made on the code is the way the coordinates of the objects in the sky are taken. Previously, the direction at which the telescope is pointing, and hence the coordinates on the celestial sphere of the object it is pointing to, were taken by measuring three angles. A vertical and an horizontal angle that were measured directly on the mount of the telescope, and also the angle between the telescope pointing direction and the north. Then these three angles were converted into Altitude and Azimuth in the code. This was unnecessarily complicated and was leading to a lot of conversions errors and uncertainty in the measurements. This was improved by using as previously mentioned the RA and DEC angles of the object, that are directly measured on the photos using the stars in the background as a reference, thanks to the website `astrometry.net` [8].

After these two modifications on the angles conventions and measurements, the code was finally tested on new pictures. Unfortunately, the code wasn't working on those new images. Many errors appeared, in particular in the image treatment, when the algorithm tries to find the satellite's trace on the image. After several weeks trying to correct and modify the code to make it run on the new images, the code

was still not working. The decision was then taken to write everything again from the beginning.

The code as it is written now uses only RA and DEC angles. The position of the satellite is measured using `astrometry.net`, as mentioned before. Also, now every information that is needed, except the location of the observer that has to be written manually on a text file, is stored in the header of the photo that is in a `.fits` format, whereas before the photo was in a `.jpg` format and every information had to be written by hand in a specific text file. While in the previous code, the whole image treatment was written mostly from scratch, which was leading to a lots of errors, the code is now written using mostly pre-existing libraries such as OpenCV [9], that have already functions that does what is needed. Theses libraries are well known and widely used, which makes it much easier to avoid mistakes and find help and documentations.

To find the satellite traces, the main steps are the following : first, since the satellite trace is the most bright and wide object on the picture, every object detected on the picture that is less bright than a certain limit and that is not covering a certain amount of pixel is taken off. If a star remains, which happens very rarely, it can be taken off by hand. Then the image is blurred to a certain level, to make the next step easier. The next step is then to draw a line on the edges of every object on the picture - at this point, the only remaining object is the satellite trace. Finally, the coordinates of the two ends of the trace are taken, thanks to the line previously drawn. This can be even improved, see Sect. 5.2 for more details.

Since the only relevant informations on the IODs (Interactive orbital determination) where the time and the angle, the specific IOD format was not necessary, and it was decided not to be used anymore. The observation time and the RA and DEC are directly written in a text file in their respective units, without any other specific format restriction. This allows the angles and date to be used with even more precision, since the number of digits used is not restricted anymore. Although this is not very useful for the angles, it allows not to round the value of the observation time to early in the code, hence reducing uncertainty.

Another difference is now the possibility to choose to use more than one image for a given satellite. Indeed, it is possible to use one image using as before the beginning, middle and end of the satellite's trace (which leads to several errors, see Sect. 5.1), or to use two photos with the beginning and end of one trace and the beginning or end of the other one, or to use three photos using beginning or end of each trace.

Finally the Gauss algorithm has been written following the same reference book [10], but this time again more pre-existing libraries were used to simplify the computations, such as the calculation of the local sidereal time for example.

All those modifications lead to better results and a faster code, that runs in about 10 to 30 seconds, while the previous code was taking more than 3 minutes for only one test image.

2.4 Gauss's method and orbital parameters

In this section, the Gauss method is developed and largely inspired by *Orbital Mechanics for Engineering Students*, chapter 5.10 [10] as well as some useful orbital parameters. Consider an object whose trajectory B is being studied (see Fig. 3). Three observations of the latter are made at three different times: t_1, t_2 and t_3. In the same figure, C denotes the center of attraction, O the observer and γ the vernal axis. To study the object's dynamics, it's needed to identify its geocentric position vector $\vec{r}_i$, $i \in \{1, 2, 3\}$ for each time. The latter depends on three quantities which are the position $\vec{R}_i$ of the observer, the distance separating the object from the observer ρ_i and the topocentric direction cosine vector $\vec{\rho}_i$. the relations describing them are given by

$$\vec{r}_i = \vec{R}_i + \rho_i \vec{\rho}_i \tag{1}$$

where $\vec{R}_i$ is defined as

$$\vec{R}_i = \left[\frac{R_e}{\sqrt{1 - (2f - f^2)\sin^2 \phi}} + H \right] \cos \phi \left(\cos \psi_i \hat{X} + \sin \psi_i \hat{Y} \right) + \left[\frac{R_e(1 - f)^2}{\sqrt{1 - (2f - f^2)\sin^2 \phi}} + H \right] \sin \phi \hat{Z} \tag{2}$$

with $R_e = 6378$ km the equatorial radius of the earth, $f = 0.003353$ the earth's flattening factor, H the altitude, ϕ the latitude, ψ_i the local sideral time (for each time) of the site and $\hat{X}, \hat{Y}, \hat{Z}$ the basis vectors of the inertial (non-rotating) equatorial frame. Note that γ denotes the vernal axis.
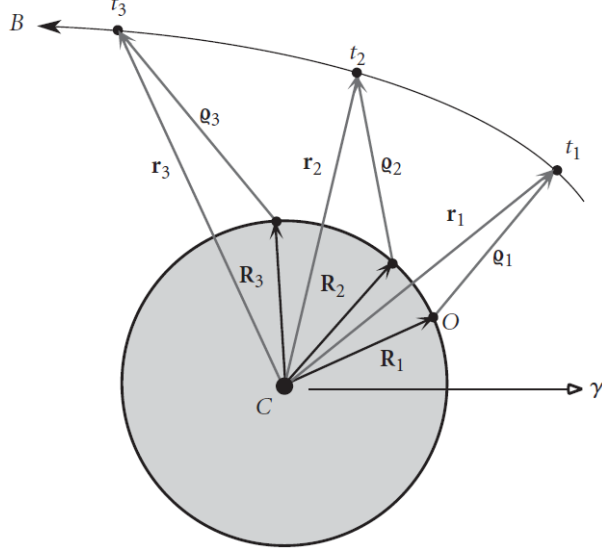

Figure 3: Schema of a trajectory B of an object viewed by an observer O with the different distances that relate them [10].

In addition, the vectors $\vec{r_i}$ must necessarily lie on the same plane because of the conservation of angular momentum. This adds a further relation to the previous equations and it reads

$$\vec{r_2} = c_1 \vec{r_1} + c_3 \vec{r_3} \tag{3}$$

where c_1 and c_3 are two constants to be determined. Introducing now the velocity $\vec{v_i}$ of the object at the three different times, the positions $\vec{r_1}$ and $\vec{r_3}$ can be expressed as a linear combination of $\vec{r_2}$ and $\vec{v_2}$ by

$$\vec{r_1} = f_1 \vec{r_2} + g_1 \vec{v_2} \tag{4}$$
$$\vec{r_3} = f_3 \vec{r_2} + g_3 \vec{v_2} \tag{5}$$

where f_i and g_i represent the Lagrange coefficient evaluated at time t_i. To find the constants c_1 and c_3, we apply the cross product to Eq. 3, then taking the scalar product and isolating these two constants it comes

$$c_1 = \frac{(\vec{r_2} \times \vec{r_3}) \cdot (\vec{r_1} \times \vec{r_3})}{||\vec{r_1} \times \vec{r_3}||^2} \qquad c_3 = \frac{(\vec{r_2} \times \vec{r_1}) \cdot (\vec{r_3} \times \vec{r_1})}{||\vec{r_1} \times \vec{r_3}||^2} \tag{6}$$

After a few algebraic steps, the two constants above can be written in terms of Lagrange coefficients as follows

$$c_1 = \frac{g_3}{f_1 g_3 - f_3 g_1} \qquad c_3 = -\frac{g_1}{f_1 g_3 - f_3 g_1} \tag{7}$$

It's important to note that if the time interval between the three observations is small, then the Lagrange coefficients can be approximated by depending only on $\vec{r_2}$. By doing so, the approximation of the latter gives for $j \in \{1, 3\}$

$$f_j \approx 1 - \frac{1}{2} \frac{\mu}{r_2^3} (t_j - t_2)^2 \qquad g_j \approx (t_j - t_2) - \frac{1}{6} \frac{\mu}{r_2^3} (t_j - t_2)^3 \tag{8}$$

where $\mu = GM_t \approx 3.986 \cdot 10^{14}$ m^{3}s^{-2} [11] and $||\vec{r_2}|| \equiv r_2$, with G the gravitational constant and M_t the Earth mass. Then, after expanding the latter expression, keeping only the terms at most of order 3 for $(t_j - t_2)$ and using binomial theorem, Eq. 7 becomes

$$c_1 \approx \frac{t_3 - t_2}{t_3 - t_1}\left(1 + \frac{1}{6}\frac{\mu}{r_2^3}((t_3 - t_1)^2 - (t_3 - t_2)^2)\right) \tag{9}$$

$$c_3 \approx -\frac{t_1 - t_2}{t_3 - t_1}\left(1 + \frac{1}{6}\frac{\mu}{r_2^3}((t_3 - t_1)^2 - (t_1 - t_2)^2)\right) \tag{10}$$

After that, ρ_i from Eq. 1 can be expressed as a function of c_1 and c_3 and using Eq. 3 it finally gives

$$\vec{r_2} = \frac{1}{f_1}\vec{r_1} - \frac{g_1}{f_1}\vec{v_2} \qquad \vec{v_2} = \frac{1}{f_1 g_3 - f_3 g_1}(-f_3\vec{r_1} + f_1\vec{r_3}) \tag{11}$$

Now, with the help of this algorithm, it's possible to determine some orbital parameters described below. The inclinaison i is given by

$$i = \cos^{-1}\left(\frac{h_Z}{h}\right) \tag{12}$$

with h and h_z the norm of the angular momentum (defined as $\vec{h} = \vec{r} \times \vec{p}$) as well as its z component. Note that $0° \leq i \leq 180°$. In order to define the eccentricity e, it's useful to define the eccentricity vector $\vec{e} = (e_x, e_y, e_z)$ as

$$\vec{e} = \frac{1}{\mu}\left(\vec{v_2} \times (\vec{r_2} \times \vec{v_2}) - \mu\frac{\vec{r_2}}{r_2}\right) \tag{13}$$

Then, the eccentricity e is simply obtained as

$$e = \sqrt{\vec{e} \cdot \vec{e}} = \frac{1}{\mu}\sqrt{(2\mu - r_2 v_2^2)r_2 v_r^2 + (\mu - r_2 v_2^2)^2} \tag{14}$$

where v_r is the radial velocity, $r_2 \equiv ||\vec{r_2}||$ and $v_2 \equiv ||\vec{v_2}||$. Another orbital parameter used is the RA (right ascension) of the ascending node Ω, for which it is necessary to introduce the node line $\vec{N} = (N_x, N_y, N_z)$ and its magnitude $N = \sqrt{\vec{N} \cdot \vec{N}}$. Then, Ω reads

$$\Omega = \begin{cases} \cos^{-1}(N_x/N) & \text{if } N_y \geq 0 \\ 360° - \cos^{-1}(N_x/N) & \text{if } N_y < 0 \end{cases} \tag{15}$$

with N_x and N_y the x and y componants of the node line. With these last quantities, it's possible to obtain the argument of perigee ω defined by

$$\omega = \begin{cases} \cos^{-1}(\vec{N} \cdot \vec{e}/Ne) & \text{if } e_z \geq 0 \\ 360° - \cos^{-1}(\vec{N} \cdot \vec{e}/Ne) & \text{if } e_z < 0 \end{cases} \tag{16}$$

with e_z the component of $\vec{e}$ along $\hat{Z}$ axis. The true anomaly θ is an important quantity to calculate the mean anomaly M. True anomaly is expressed as

$$\theta = \begin{cases} \cos^{-1}(\vec{e} \cdot \vec{r}/er) & \text{if } v_r \geq 0 \\ 360° - \cos^{-1}(\vec{e} \cdot \vec{r}/er) & \text{if } v_r < 0 \end{cases} \tag{17}$$

Thus, M is directly given by [12]

$$M = \text{atan2}\left(-\sqrt{1 - e^2}\sin\theta, -e - \cos\theta\right) + \pi - e\frac{\sqrt{1 - e^2}\sin\theta}{1 + e\cos\theta} \tag{18}$$

where atan2 is a Python function which gives for a couple $(x, y) \in \mathbb{R}^2$ the angle between the line joining the origin $(0, 0)$ and (x, y) and the x-axis in the Cartesian plane. In addition, the mean motion n is given by the following expression [13]

$$n = \sqrt{\frac{\mu}{a^3}} \tag{19}$$

where a denotes the semi major axis of the object's elliptical trajectory. The semi-major axis is calculated as

$$a = \frac{1}{2}(r_a + r_p) \tag{20}$$

where r_a and r_p are the apogee and perigee radii, respectively. These are defined as

$$r_a = \frac{h^2}{\mu}\frac{1}{1 + e\cos(0)} = \frac{h^2}{\mu}\frac{1}{1 + e}, \qquad r_p = \frac{h^2}{\mu}\frac{1}{1 + e\cos(\pi)} = \frac{h^2}{\mu}\frac{1}{1 - e} \tag{21}$$

Finally, it's necessary to define the relative variation (in percent) ϵ of an orbital parameter α given by

$$\epsilon = \frac{|\alpha_{\text{var}} - \alpha_0|}{|\alpha_0|} \times 100 \tag{22}$$

where α_{var} denotes the orbital parameter given by Gauss algorithm without modifying the input and α_{var} is the same orbital parameter given by the algorithm with a input that has been modified.

2.5 Verification of Gauss algorithm

Before applying this implementation to concrete data, it is worth carrying out a few numerical checks on fictitious examples. These are taken from the book *Orbital Mechanics for Engineering Students* [10]. More specifically, the verification of the Gauss algorithm is carried out in two stages. First, we check Eq. 1 to 11, and in particular whether the state vectors $\vec{r}_2$ and $\vec{v}_2$ are consistent. These are the basis for determining the orbital parameters needed to reconstruct an orbit. To do this, let's consider the fictitious situation, taken from [10], where a tracking station, located at a northern latitude of 40° and at an altitude of 1 km is observed. A summary of the initial data is given in Tab. 1. Note that the state vectors $\vec{r}_2$ and $\vec{v}_2$ obtained with the implementation of the Gauss algorithm are also presented, as are the reference values found in [10].

Observation	t [s]	RA [°]	Declination [°]	Local sidereal time θ [°]
1	0.00	43.437	-8.783	44.506
2	118.10	54.420	-12.074	45.000
3	237.58	64.318	-15.105	45.499

Vector state comparison	Experimental	Reference
$\vec{r}_2$	$5646.3\hat{I} + 6516.1\hat{J} + 3274.1\hat{K}$	$5659.1\hat{I} + 6533.8\hat{J} + 3270.1\hat{K}$
$\|\vec{r}_2\|$ [km]	9222.8	9241.8
$\vec{v}_2$	$-3.8846\hat{I} + 5.0334\hat{J} - 2.2085\hat{K}$	$-3.9080\hat{I} + 5.0573\hat{J} + -2.2222\hat{K}$
$\|\vec{v}_2\|$ [km/s]	6.73	6.76

Table 1: Comparison of the state vectors $\vec{r}_2$ and $\vec{v}_2$ obtained by the Gauss algorithm with the reference values obtained in [10].

It can therefore be observed that the results obtained using Gauss's algorithm and those presented in [10] seem to be in agreement. Indeed, the relative error between the norm of the vector $\vec{r}_2$ obtained by the Gauss algorithm and the norm of the vector $\vec{r}_2$ supplied as a reference is of the order of 0.2% as for the relative error on the norm of the velocity vector $\vec{v}_2$, this is of the order of 0.4%. Note that the slight differences observed in Tab. 1 are essentially due to rounding errors in [10].

3   Experimental setup

3.1   Celestron RASA-36 telescope and camera

Observations of the satellites orbiting the Earth were made using the Celestron Rowe-Ackermann Schmidt Astrograph (RASA) 36 telescope (see Fig. 4). It consists of a main mirror with a diameter of 35.5 cm. The light reflected from the satellites is reflected by this main mirror onto a series of lenses at the front of the telescope. This series of lenses is used to focus the reflected light onto a camera sensor, located at the front of the camera. The camera, also attached to the front of the telescope, is shown in Fig. 12 in Sect. 7.1. In addition, the focal length of the telescope is 795 mm. During observations, the telescope is mounted on a mount to compensate for the Earth's rotation. Note that the mount also has go-to and sky tracking capability, i.e. the ability to tell the mount where in the sky to point the telescope. Finally, as mentioned above, a camera is also present on the front of the telescope. This is a ZWO ASI 2600 MM Pro monochrome camera, whose sensor has a resolution of (6248x4176) pixels. The sensor size is 23.5 mm×15.7 mm and it has a brightness level per pixel of 65536. Note that to avoid thermal noise during long exposures, the camera can be cooled thanks to Peltier effect and a ventilator [14].

Associated with the telescope, the Celestron PWI (CPWI) Telescope Control Software allows it to be controlled from a computer [15]. When opening the software on the computer, a map of the sky opens and with the help of a cursor, it's possible to point the telescope in the desired direction. Note that this can only be done after calibration of the latter, which will be explained in Sect. 3.3.

Figure 4: The RASA telescope on a rooftop at EPFL campus.

3.2   Satellite tracking

As explained above, the light reflected from the satellite is captured by the telescope. In addition, due to the high speed of the satellites orbiting the Earth, compared to the exposure time, a trace left by the satellite appears. In order to obtain images of the best possible quality, it is important to take into account the following facts: the visibility of satellites is best shortly after sunset. Furthermore, in order to obtain good quality images, it is necessary to reduce light pollution as much as possible. The Astroval observatory in the Vallée de Joux is the ideal place for this purpose. Nevertheless, many images were taken on the EPFL campus, from the roof of the ELG building. Finally, it is obviously necessary that the sky is free of clouds in order to obtain quality images.

3.3   Experimental method

In this section, the strategy adopted to take a picture of a space object's track using the telescope will be explained.

After mounting the telescope, it must first be calibrated as it does not know its GPS location. To do this, it is necessary to visually locate Polaris and point by hand the telescope in its direction. This first step is necessary because the latter is aligned with the Earth's axis of rotation (which is why it is always seen towards the North), which gives a first axis reference. Note that it is not necessary for the telescope to be aligned with Polaris with extreme precision, the fact that Polaris is in the field of view of the telescope at the time of calibration is enough to make measurements. In addition, the mount of the telescope allows a rotation of this one according to two angles, the calibration towards Polaris also allows these two angles to be synchronized with the rotation of the Earth. Then, the telescope needs to know the spatial scale of the sky, i.e. the differences in angles between the various celestial objects. To do this, three sufficiently distant stars will be chosen and with the help of the software CPWI, the

telescope is pointed towards them successively.

To detect the satellites, the mobile application "Heavens-Above" was used to determine their position in real time. By knowing the user's GPS position, this application visually displays the constellations and satellites visible from that position. An example is given in Fig. 5a. In this picture, it can be seen the satellite named "RS-15", and its visible orbit is represented by the curved red arrow. The trajectory of the latter will pass through the constellation of Drago and more precisely close to the star Tyl which is situated in the middle of the white circle on this same figure. Knowing this, it is possible to point the telescope (before the satellite passes by) towards this star using the associated CPWI software. This is shown in Fig. 5b which illustrates this software around the Drago constellation. The yellow cursor is placed precisely on the star Tyl.
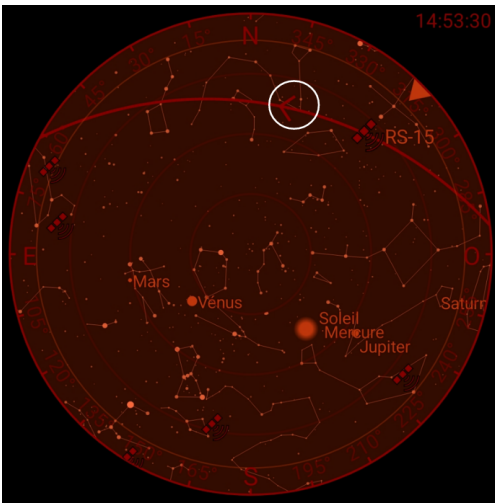
(a)   (b)

Figure 5: (a) Visualisation of a satellite orbit on the "Heavens-above" application (b) Zoom in the CPWI software on the Drago constellation.

Once the telescope is oriented in the desired direction, the trace of the object under study is obtained by taking long exposure images with an exposure time of 0.5 s. Since most of the debris and satellites are in low earth orbit, a longer exposure time would have meant that the images would not contain the entire track, i.e. the beginning and end of the track would not be visible on the images. However, these are important aspects when the analysis of the track is carried out via algorithms. In addition, in order to be sure of obtaining the desired track at the right time, a series of long-exposure images is voluntarily launched a few tens of seconds before the object passes through the point where the telescope is pointed on the "Heavens-Above" application. An example of a long exposure image is given in Fig. 6. It was taken with the RASA telescope on the evening of 2 May 2023 on the roof of the ELG building from the EPFL campus.

Figure 6: Track of the Starlink 3935 satellite taken on the 2nd May 2023 from the EPFL campus.

4   Results

During the observations, various satellites were selected in order to determine their TLEs and compare them with a database. In this respect, the Starlink satellites represent a satisfactory and reliable

source of data. As a result, the TLEs of the satellites Starlink-1259/1296/3965/3948, obtained with one trace on one image, and the Starlink-1589, obtained with traces on two images, were determined and compared with reference values [7] (see Tab. 2). The TLEs obtained for the Starlink-1589 is shown in Fig. 7. Note that the Starlinks-1259/1296/3948 and 3965 satellites were observed on Tuesday 2 May 2023 at 20:56:39.702, 21:07:37.835, 20:30:46.588 and 20:42:24.422 UTC, respectively, while the Starlink 1589 satellite was observed on Friday 26 May 2023 at 21:44:02.813 UTC.

Starlink number	Type of TLEs	i [°]	Ω [°]	e	ω [°]	M [°]	n [day^{-1}]
1259	Experimental	27 ± 3	129 ± 11	$1.5730 \cdot 10^3$	267 ± 7	NaN	37 ± 3
	Reference	53	134	0.0001	93	266.4833	15
1296	Experimental	84 ± 6	214 ± 10	$2.6162 \cdot 10^6$	225 ± 5	NaN	NaN
	Reference	53	134	0.0001	91	269.0430	15.0639
3965	Experimental	54 ± 5	158 ± 8	$2.1510 \cdot 10^3$	74 ± 6	NaN	32 ± 3
	Reference	53	126	0.0001	68	291.1716	15
3948	Experimental	59 ± 6	148 ± 8	$2.2370 \cdot 10^4$	69 ± 5	NaN	NaN
	Reference	53	127	0.0001	45	314.7218	15.0906
1589	Experimental	48 ± 3	144 ± 12	0.9960	258 ± 10	2 ± 2	48 ± 4
	Reference	53	160	0.0001	79	280.3882	15

Table 2: Comparison of the TLEs obtained experimentally with the reference TLEs taken from [7].

```
0 STARLINK-1589 :
1 00000U 00000A   23146.90560237  .00000000  00000-0  00000-0 0  0000
2 00000  47.6754 144.2419 9960040 257.9511   1.6442 48.16593123000000
```

Figure 7: TLE obtained from the observation of the starlink-1589 at 21:44:4.045 UTC on the 26th of may 2023 [7].

Now that the various comparisons between the TLEs obtained experimentally and those obtained from the SpaceTrak database have been carried out, the relative errors can be quantified. This is carried out for each satellite observed and is shown in Tab. 3.

Relative error on	i	Ω	e	ω	M	n
Starlink 1259	49 %	4 %	–	187 %	–	147 %
Starlink 1296	58 %	60 %	–	147 %	–	–
Starlink 3965	2 %	25 %	–	9 %	–	113 %
Starlink 3948	11 %	17 %	–	53 %	–	–
Starlink 1589	11 %	10 %	–	225 %	–	220 %

Table 3: Relative error calculated between the orbital elements obtained experimentally and those of reference, obtained according to [7].

Note that, since the eccentricity $e > 1$ for the Starlink-1259/1296/3965 and 3948 satellites, the mean anomaly M is not defined (see Eq. 18). Furthermore, according to Eq. 20 and 21, it can also be seen that when $e > 1$, i.e. for the same Starlink satellites, the semi-major axis a can become negative. As a result, according to Eq. 19, the mean motion n is no longer defined in this case. This situation corresponds to the Nan values in Tab. 2.

In addition, the large difference in order of magnitude between the eccentricities obtained experimentally and the reference values presented in Tab. 2 suggests relative errors that are physically irrelevant. As a result, these have been omitted from Tab. 3. As developed previously, and in agreement with Eq. 18 and 19, the mean anomaly and mean motion depend directly on the eccentricity calculation. The relative errors concerning these quantities have therefore also been omitted, in cases where they

are physically irrelevant.

Once the TLEs had been obtained and compared with the reference values, further analyses were carried out. In particular, the times t_i taken as input by the Gauss algorithm are modified to better understand the temporal dependance for certain orbital parameters. Note that the Starlink-1589's TLE has been chosen in this analysis (see Tab. 2). Fig. 8a and 8b illustrates the angular variation and the relative variation ϵ (in percent, see Eq. 22) for the orbital parameter Ω and i, Ω, e, ω, n, respectively. The results for the orbital parameter M were absurd and hence they are not presented in the following results. Note that on Fig. 8b, the orbital parameters obtained with respect to these time modification are represented by a black star ($+1$s), a blue circle ($+0.5$s) and a red cross (-0.3s). On Fig. 8a, the value of Ω after modifying the time intervals Δt_i are represented by the black crosses while the initial value, i.e when there is no time modification in the input, is represented by the red cross. In addition, Fig. 8c represents the relative variation ϵ (in percent) of the orbital parameters i, Ω, e, w, n when the times in the Gauss algorithm input is shifted by $+1$s (blue circle) and -1s (red cross).
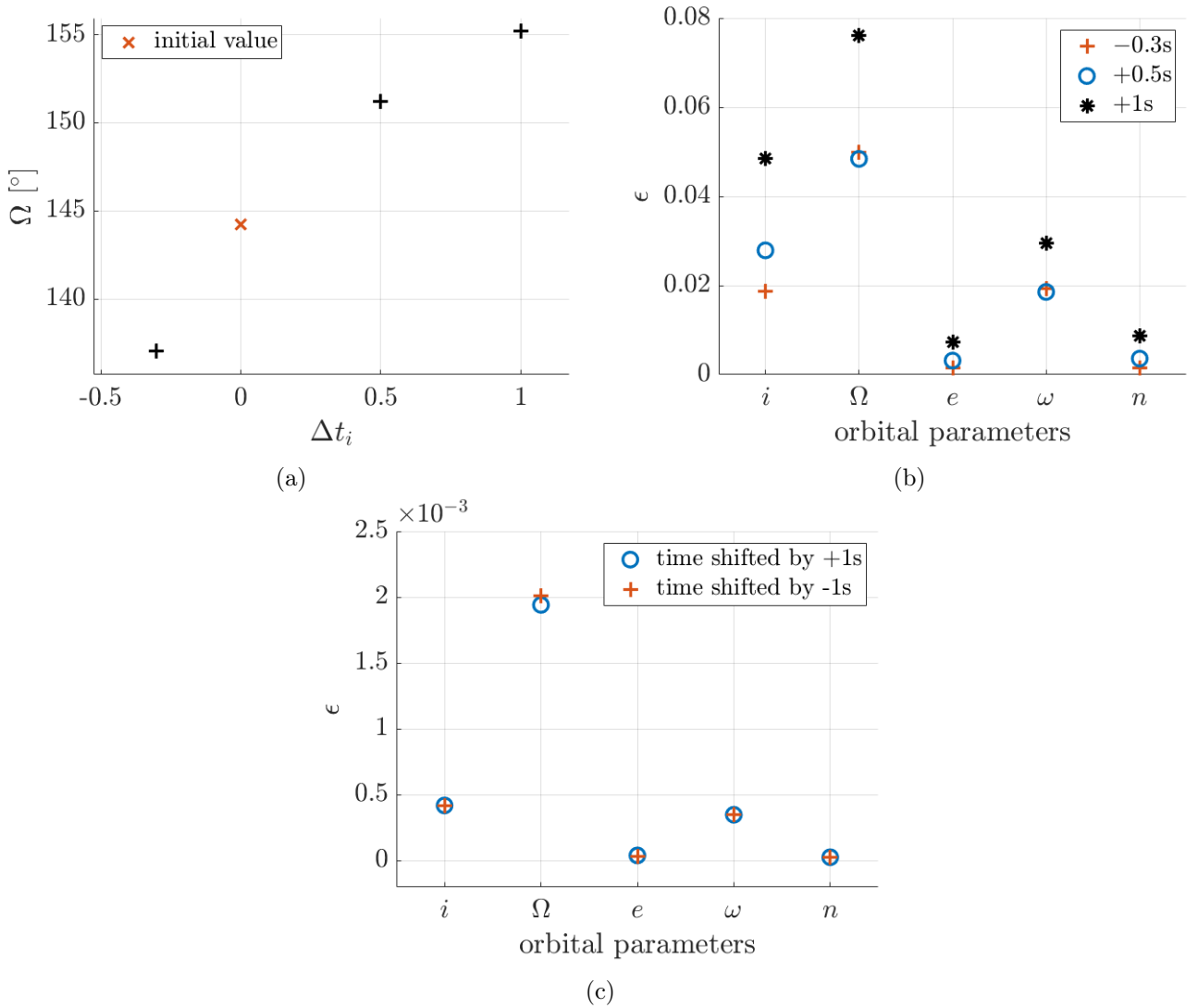

(a)

(b)

(c)

Figure 8: (a) Illustration of the angle of the orbital parameter Ω (b) and the relative variation of i, Ω, e, ω, n by modifying time intervals adding -0.3s, 0.5s and 1s to the input (c) Relative variation of i, Ω, e, w, n by shifting the times input by $+1$s and -1s

The same method has been carried out varying this time the Right Ascension and the Declination in input, to see the influence of these parameters on the obtained TLEs. The results are shown in Fig. 9a, 9b, 9c and 9d and represent the relative variations of the orbital parameters in percent. In

Fig. 9a, the declination have been manually modified in input in the following way : in case a, the DEC of the first of the three points used as an input to compute the TLE has been shifted by -15 arcminutes, while the DEC of the third point has been shifted by +15 arcminutes. This has been made because 15 arcminutes is a large estimation of the uncertainty on the measure of the DEC. The way the DEC is shifted in opposite directions for the first and third point is supposed to simulate the worst case scenario where the direction of the trace used by the algorithm and the actual direction of the trace differ the most. In case b, the first DEC is shifted by +15 arcminutes while the third is shifted by -15 arcminutes. The Fig. 9b, the same experiment has been done, with case a and b corresponding exactly to the same cases a and b respectively of the Fig. 9a, but this time, since the RA is in hour angle, the RA is shifted by 1min (which is equal to 15 arcminutes). The Fig. 9c and Fig. 9d shows the relative variations of the orbital parameters when the three DEC and RA respectively are shifted by ± 15 arcminutes and ± 1 min respectively.
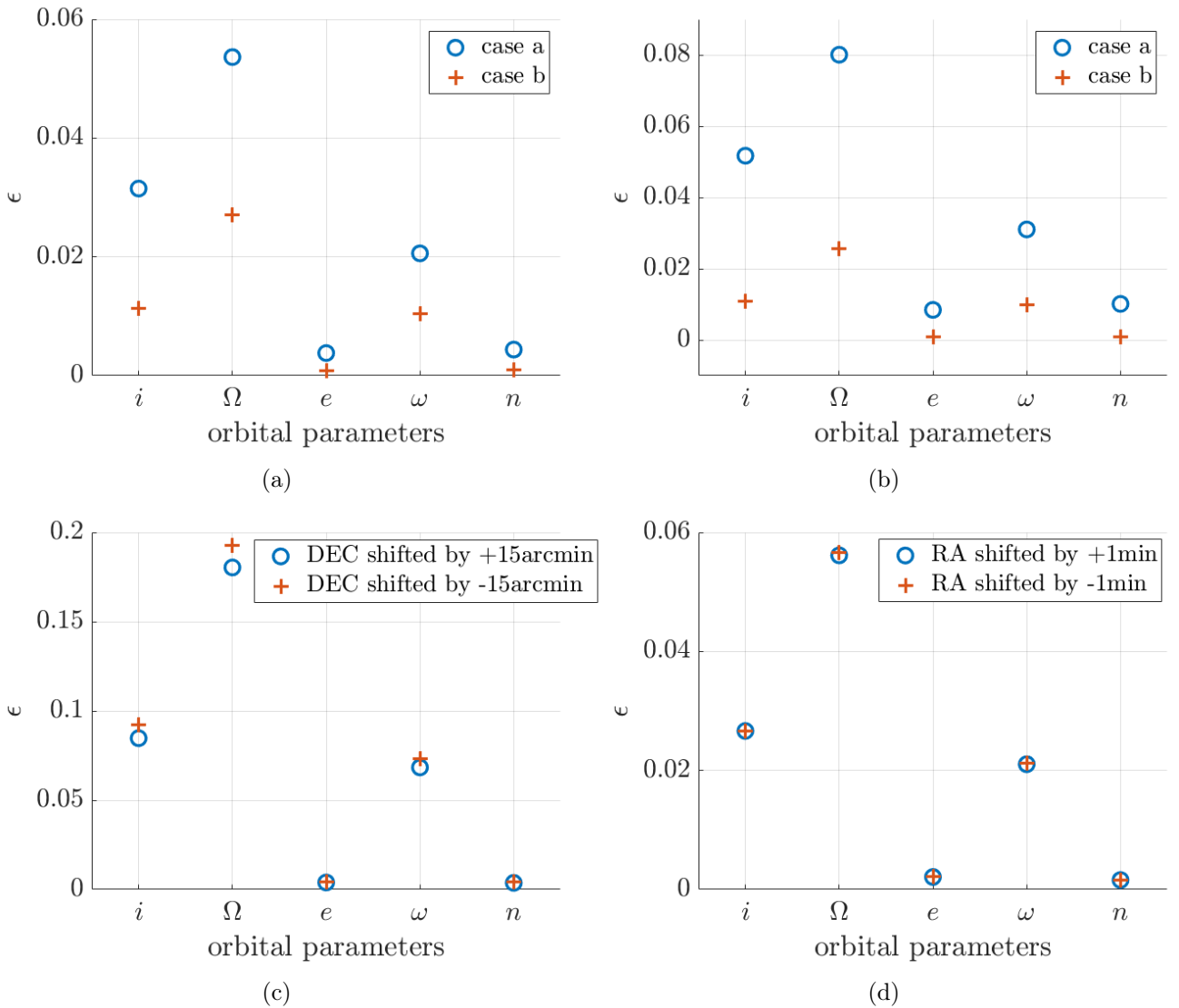

Figure 9: Relative variations of the orbital parameters when varying in input (a) the DEC of first and third point in opposite way, (b) the RA of first and third point in opposite way, (c) the DEC of the three points uniformly, (d) the RA of the three points uniformly.

5   Discussion

5.1   Results analysis

As developed in Sect. 4, Tab. 2 and 3 represent the various orbital parameters necessary for the reconstruction of an orbit, compared with the reference orbital parameters obtained according to [7], as well as their relative errors, respectively. It should also be remembered that the NaN values are justified in the sense that the mean anomaly M and the semi-major axis a are not defined in the limit where the eccentricity $e > 1$. The key elements in analysing these results are therefore present in Tab. 3. It should first be noted that for satellites observed using a single track (Starlink-1259/1296/3965/3948), the relative errors are variable. In fact, for the Starlink-3965 satellite, the inclination i and the right ascension of the ascending node Ω, the relative errors seem reasonable insofar as they vary between 2 % and 25 %. Nevertheless, these values do not allow to state that determining orbital parameters using a single trace is a good method. On the contrary, the relative errors on i and Ω for the Starlink-1259/1296 and 3948 satellites range from 4 % to 60 %. Note also that the fact that $e > 1$ is systematically present also suggests that determining the orbital parameters using only one trace is unwise (see Tab. 2). This argument is supported by the fact that for the Starlink-1589 satellite, an eccentricity $e < 1$ is obtained.

In fact, when taking only one image, the second point is set to be the middle of the trace, for a time exactly in the middle of the exposure time. This is in general not true, as one can see on the Fig. 10. The red line is the part of the orbit covered by the satellite when the observer sees an angle of 45° between the beginning and the end of the trace, near the horizon. The blue line is the part of the orbit covered by the satellite when the observer sees an angle of 45° between the beginning and the end of the trace, near the Azimuth. As one can see, the red line is longer than the blue line. This means that if the satellite has an almost constant velocity, it takes more time to cover the red part than the blue one. This means that when taking a picture of a satellite, the satellite is not in the middle of the trace in the middle of the snapshot's exposure time. Then the eccentricity has to be very high in order to calculate an orbit that passes through the three points of the trace.
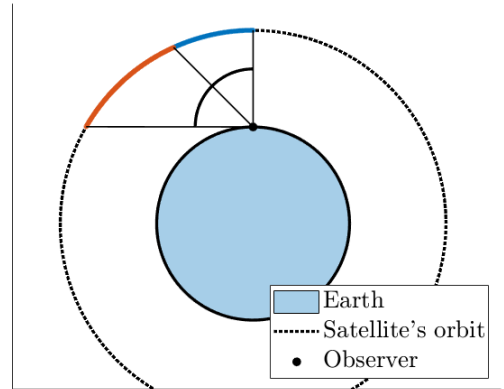

Figure 10: Scheme that illustrates the difference between the angle seen by the observer and the actual distance covered by the satellite.

The aim of Fig. 8a, 8b and 8c is to analyse the time dependence of different orbital parameters. As a reminder, Fig. 8a and 8b are obtained by modifying the time intervals by a quantity of -0.3s, +0.5s and +1s, while a shift of +1s and -1s is applied to the time inputs for Fig. 8c. Only Ω is represented in Fig. 8a because it's the parameter that undergoes the most variation after modifying the input time. The angle differences between the initial value and the modified values are 7.2°, 6.9° and 10.9° for modifications -0.3s, +0.5s and +1s, respectively. Assuming in absolute terms that the time changes of -0.3s and +0.5s are too close to observe a difference in the deviations of the resulting angles, it seems that the greater the time change in the input, the greater will be the change in angle. For Fig. 8b, the relative variation in orbital parameters (see Eq. 22) compared with their unmodified value is studied here. The first observation is that for all the orbital parameters, the relative variation is the highest when the time correction in the input is +1s (black star). For this correction, the largest relative variation is the one associated with Ω whose value is $\epsilon = 0.076\%$ and the smallest, associated with e, is $\epsilon = 0.007\%$. In addition, it can be seen that ϵ increases as the value of the time correction input increases (in absolute terms). This behaviour is observed for i, e and n. In the case of ω and Ω, the relative variations obtained for corrections -0.3s and +0.5s are very close to each other. It can be argued that since the difference is small, a pattern similar to the other parameters is envisaged.

Fig. 8c shows the relative variation ϵ of the orbital parameters i, Ω, e, ω and n after changing the time in the input. However, it's now the independent times that are shifted by $+1$s (blue circle) and -1s (red cross) and not the time intervals as before. In this case, the order of the relative variation is $10^{-3}\%$, which means that the time shift modifies the angles very little. In addition, it's clear that no difference is visible between a shift of ± 1s. It should nevertheless be noted that for Ω, the -1s time shift generates a slightly higher relative variation than the $+1$s shift. However, as the difference between the two is $6.9 \cdot 10^{-5}$ %, the difference can be neglected.

Fig. 9a, 9b, 9c and 9d shows the results obtained when varying the input values of the Right Ascension and the Declination. First thing one can see on Fig. 9a and Fig. 9b is the fact that the results are asymmetrical : for example the relative variation of the inclination in Fig. 9a is greater by 0.02% in case a than in case b. Same goes for the other parameters ; the values obtained in both Fig. 9a and Fig. 9b are greater in case a. This is mainly caused by the fact that the Starlink-1589 satellite trace on the picture used, the angle between the trace and the DEC axis is not the same as the angle between, the trace and the RA axis. So when varying one parameter while keeping the other constant, this lead to asymmetrical modifications.The Fig. 11 illustrate this fact. As one can see on Fig. 11, the angle of the red line (illustrating case b) and the satellite initial trace in black is smaller than the angle between the blue line (illustrating case a) and the satellite initial trace in black.So the red trace is closer

Figure 11: Scheme that illustrate as an example the different traces when varying RA while keeping DEC constant.

to the black one, hence the results are less modified by the variation made.In both Fig. 9a and Fig. 9b, the relative variation is the greater for the parameter Ω, which is at most about 0.05% when varying DEC, and 0.08% when varying RA.This represent an absolute difference of about 12 degrees on the absolute value when varying the RA, going from $\Omega = 144°$ to $\Omega = 155°$. The parameters e and n are the parameters that vary the less. For all the other parameters, the relative variation varies from 0.01% to 0.05%. In general, the relative variations are small for all parameters.

The Fig. 9c and Fig. 9d shows the variations of the orbital parameters when the RA and DEC respectively are shifted the same way for the three points. It can be seen that the relative variations are small for all parameters. Ω is again the parameter that varies the most, with a relative variation of 0.06% when varying the RA.
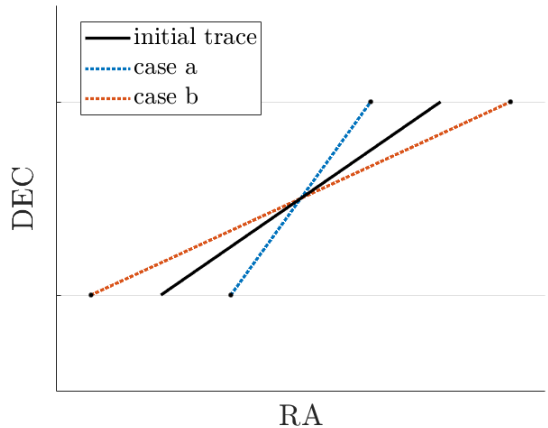
In both Fig. 8 and Fig. 9, one can see that the relative variations are very small for all parameter. However, the results are far from the references, as one can witness in the Tab. 2 and Tab. 3. This may be explained by the fact that since the results are far from the real values, varying the parameters leads to an error of the same order of the initial value. Hence, when subtracting the two values, the difference is then very small compared to the magnitude of the initial value, which makes the ratio of the difference and the initial value very small. This may explain why despite very small relative variations, the values are still off.

5.2 Possible improvements

First of all, the main source of uncertainty is the measurement of the time. If the time measurement is not accurate enough, the position of the satellite in the sky is not well determined. In fact, the position calculated depends on the angle at which the observer sees the satellite. These angles depends

on the position of the observer on earth in the reference frame of the static stars, which means that the way the angles are used to calculate the position of the satellite also depends on the time at which the photo is taken. Also, the time dependence also directly appears in the calculation of the satellite speed, which then propagates into the satellite altitude and the shape of the orbit. So the time measurement is the most crucial one. Unfortunately, in this work the time measurement where made with the time of the computer, which may be precise enough but is very likely to be slightly offset. The duration measurements are probably not accurate enough, as well as the absolute time. This is certainly the main reason the results are not as close as desired. A way to improve this could be the use of GPS time synchronization.

The use of multiples photos of the same satellite will also certainly improve the results. As discussed before, taking only one image is probably not working at all. Getting three points from two images is already an improvement, as well as taking three points with three images. However, the orbit calculated for the satellite will passes through the three points. This means that if the three points are not calculated perfectly on the almost circular true orbit of the satellite, the calculated orbit has to be very eccentric in order to create an ellipse that passes through the three points. This may be improved by taking more than three points, which means taking more photos, and by then calculating the orbit that fits the most but does not necessarily passes through all the points, similarly one may do in a context of a fitting curve on a cloud of points.

The measurements of the angles, i.e. the RA and the DEC of the satellite may also be improved. This may be done with small modifications in the code. In fact, to find the three points, the image is treated as briefly explained in Sect. 2.3. In order to simplify the treatments and avoid even more errors, one could subtract in the first place a picture of the same region in the sky without the satellite's trace to the photos where there is a trace. This kind of photos are already taken anyway just before or just after the passage of the satellite on the view field of the telescope. This will in principle already take off all the objects on the image that are not the trace. Then, instead of taking the one point as exactly the edge of one trace's end, one can take the point in the center of a circle with diameter the width of the trace, with the edges of the circle superimposed on the edge of the trace. Theses improvements however will not make as significant changes as an improvement on the time measurements.

Another improvement that is also related to the code is that at some point in the calculations, it is needed to find the root of a polynomial with degree 8, and with high coefficients. This leads to non negligible numerical errors. As an example, on one on the tested images, when the root found is injected in the polynomial, the value is of the order of 10^{14}, instead of zero. This is due to the fact that the slope of the polynomial near the root is very high, hence a very small difference in the approximate root leads to a very high difference in the value of the evaluated polynomial. Several method of root optimization have been tried, none of them provided satisfying results.

6 Conclusion

In conclusion, several experiments were carried out throughout the course of this work. Firstly, using the Gauss algorithm, the orbital parameters of certain satellites were obtained from images taken by the RASA telescope (see Tab. 2). Two methods were tried, using only one or two images. It has been shown that using only one image is not enough. A study of the influence of the time and angles input on the calculated orbital parameters has been carried out. The lack in accuracy on the time measurement has been shown. Finally, the determined orbit is two sensitive to the only three points used. In order to have a good enough orbit, one needs to use more photos and hence the Gauss algorithm is not adapted for this problem.

References

[1] NASA, *James Webb Space Telescope*, last updated : Oct. 20, 2021, https://www.nasa.gov/mission_pages/webb/about/index.html

[2] The European Space Agency, *Un nouveau satellite météorologique révèle des images spectaculaires de la Terre*, May 2023, https://www.esa.int/Space_in_Member_States/France/Un_nouveau_satellite_meteorologique_revele_des_images_spectaculaires_de_la_Terre

[3] The European Space Agency, *Space debris by the numbers*, last updated : March 27, 2023, https://www.esa.int/Space_Safety/Space_Debris/Space_debris_by_the_numbers

[4] J. Barentine, A. Venkatesan, J. Heim, J. Lowenthal, M. Kocifaj, S.Bará, *Aggregate effects of proliferating low-Earth-orbit objects and implications for astronomical data lost in the noise*, nature astronomy 7, 252-258, 2023, https://doi.org/10.1038/s41550-023-01904-2

[5] A. Labarbe , A. Schwab, P. Gigon, *Orbit Interpolation from Optical Observations*, SSA EPFL TEAM, 2023

[6] A. Mukundan, H. Wang, *Simplified Approach to Detect Satellite Maneuvers Using TLE Data and Simplified Perturbation Model Utilizing Orbital Element Variation*, applied sciences, MDPI, 2021

[7] SPACE-TRACK , *Retrieve ELSET Data by Satellite Catalog Number*, Element Set (ELSET) Data, https://www.space-track.org/#gp

[8] Astrometry.net, last visited on 25 Mai 2023, https://astrometry.net/

[9] OpenCV python package, https://pypi.org/project/opencv-python/

[10] H. Curtis, *Orbital Mechanics for Engineering Students*, chap 5.10, Elsevier aerospace engineering series, 2005

[11] Jet Propulsion Laboratory, *Astrodynamics Parameters*, California Institute of Technology, NASA, 2023, https://ssd.jpl.nasa.gov/astro_par.html

[12] Wikipédia, *Mean anomaly*, last visit : May 2023, https://en.wikipedia.org/wiki/Mean_anomaly

[13] Wikipédia, *mean motion*, last visit : May 2023, https://en.wikipedia.org/wiki/Mean_motion

[14] PIERRE ASTRO, boutique, caméras astronomiques, caméras ciel profond, last visit on 20th of May 2023, https://www.pierro-astro.com/materiel-astronomique/cameras-astro/cameras-ciel-profond/camera-refroidie-monochrome-asi2600mm-pro-zwo_detail

[15] CELESTRON, *Celestron PWI Telescope Control Software*, last visit : May 2023, https://www.celestron.com/pages/celestron-pwi-telescope-control-software

[16] Heavens-Above, screenshot taken the 5th of May 2023

7 Appendix

7.1 Camera

The Fig. 12 is a photo of the camera used to take pictures with the telescope.

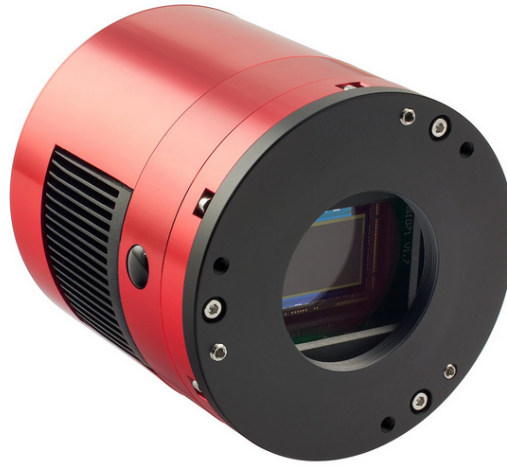Figure 12: The ZWO ASI 2600 MM Pro monochrome camera [14]

7.2 RA DEC scheme

The Fig. 13 is a scheme from [10] that illustrates the Right Ascension and the Declination of an object on the celestial sphere. γ is the vector pointing from the center of the Earth to the vernal point.
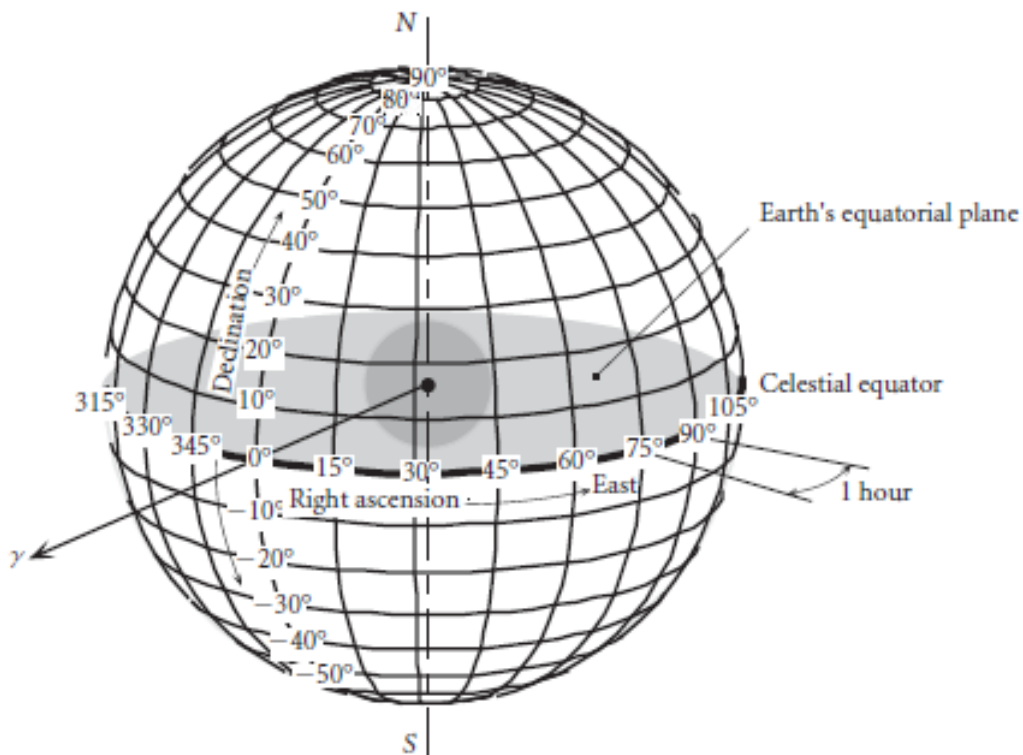

Figure 13: Scheme illustrating RA and DEC [10].

7.3   IOD format

The previous code was seperated in two parts. The aim of the first part was determining the IOD (Interactive Orbit Determination) from an input image. These IODs where then used to determine the TLE of the observed satellite. The IOD's have the following format :

00000 03 123XYZ 0000 G YYYYMMDDHHMMSSsss 00 45 DDDMMSSs+DDMMSSs 00 B+MMm
Mm SSSsss

where YYYYMMDDHHMMSSsss gives the year, the month, the day, the hour, the second and the millisecond of the observations (UTC time), respectively. DDDMMSSs+DDMMSSs gives the azimuth and the elevation angles of the satellite with D degrees, M arc minutes and S arc seconds. Once the IODs have been determined, they are passed on as input to the Gauss and Laplace algorithms. Note that the exact position of the observer must also be provided as input to the Gauss and Laplace algorithms. which are intended to interpolate the orbit of the observed object. Note that these algorithms were developed in projects prior to the project discussed in this report [5].